J Mol Model (2013) 19:4443–4457
DOI 10.1007/s00894-013-1923-8

ORIGINAL PAPER

Molecular modeling studies give hint for the existence of a symmetric hβ_2R-G$\alpha\beta\gamma$-homodimer

Andrea Straßer · Hans-Joachim Wittmann

Received: 19 February 2013 / Accepted: 16 June 2013 / Published online: 8 August 2013

Abstract Several experimental studies suggest that GPCR dimers or oligomers may play an important role in signal transduction. In 2011 the crystal structure of a hβ_2R-G$\alpha\beta\gamma$-complex was published and crystal structures of GPCR dimers are known. But until now, no crystal structure of a GPCR dimer including the G$\alpha\beta\gamma$-complex is available. In order to obtain detailed insights into interactions within hβ_2R dimers including the G$\alpha\beta\gamma$-complex we performed a potential-energy-surface scan in order to identify favored asymmetric and symmetric hβ_2R-G$\alpha\beta\gamma$-homodimers. This potential energy surface scan suggests, besides the existence of asymmetric dimers, the existence of a symmetric hβ_2R-G$\alpha\beta\gamma$-homodimer with a TM I/VII-contact. A subsequent 20 ns MD simulation of the symmetric homodimer revealed large asymmetric conformational changes of both hβ_2Rs, especially regarding TM VII and the interaction network between Asp$^{2.50}$, Val$^{7.44}$, Ser$^{7.46}$ and Tyr$^{7.43}$. Since similar conformational changes were not observed during the molecular dynamic simulation of the monomeric hβ_2R-G$\alpha\beta\gamma$-complex, it may be suggested that the conformational changes in the symmetric homodimer are related to the presence of the second hβ_2R-G$\alpha\beta\gamma$-complex. Due to the limitations of simulation time, conformational changes within a time scale of μs or ms may of course not be observed. However, the detected conformational changes, especially in TM VII, correspond to minima on the potential energy surface and thus, this study gives new insights into GPCR dimers on molecular level and furthermore, gives suggestions for site-directed mutagenesis studies.

Keywords Active state symmetric GPCR dimer · Adrenergic beta 2 receptor · GPCR dimers · Molecular dynamics · Potential energy surface scan

Introduction

The human adrenergic beta 2 receptor (hβ_2R) holds the role of a kind of "standard" receptor within the biogenic amine receptors, belonging to family A of G protein-coupled receptors [1]. Due to this "standard role", a large number of studies in literature address the hβ_2R [2–4]. In 2007, the first crystal structure of the hβ_2R was published [5] and during the following years, a lot of crystal structures of hβ_2R in an inverse agonist- or agonist-bound state, were published [6–11]. However, until 2010, the agonist-bound crystal structures were not cocrystallized with the G$\alpha\beta\gamma$ subunit. But for the active state GPCRs, this interaction is essential, with respect to the signal cascade [12–14]. Until 2010, several pharmacological and computational studies, addressing the interaction sites between the GPCR and the corresponding Gα subunit were performed [12–22]. To gain a deeper insight into interaction between the hβ_2R and Gα-subunit, in 2010 a potential energy surface scan, combined with molecular dynamic simulations

Andrea Straßer and Hans-Joachim Wittmann contributed equally to this work

Electronic supplementary material The online version of this article (doi:10.1007/s00894-013-1923-8) contains supplementary material, which is available to authorized users.

A. Straßer (✉)
Department of Pharmaceutical and Medicinal Chemistry II, Faculty of Chemistry and Pharmacy, University of Regensburg, Universitätsstraße 31, 93040 Regensburg, Germany
e-mail: andrea.strasser@chemie.uni-regensburg.de

H.-J. Wittmann
Faculty of Chemistry and Pharmacy, University of Regensburg, Universitätsstraße 31, 93040 Regensburg, Germany

was performed to predict a $h\beta_2R$-Gα-interaction model [23]. In 2011, the crystal structure of the $h\beta_2R$-Gαβγ-complex, artificially cocrystallized with Nb25 and T4-lysozyme was published [11]. A comparison of one predicted $h\beta_2R$-Gα-model with the corresponding parts of the $h\beta_2R$-Gαβγ-crystal structure revealed a rmsd of about 8.4 Å [24].

Within the last years, an increasing number of experimental and theoretical studies suggest the existence of GPCR dimers [25–41]. Furthermore, a database, addressing GPCR oligomerization is available online (http://data.gpcr-okb.org/gpcr-okb). In general, at least two models for receptor–G protein–homodimers are discussed in literature: On the one hand, asymmetric receptor–G protein homodimers, where a GPCR-homodimer interacts with only one Gαβγ-heterotrimer (Fig. 1) and on the other hand, symmetric receptor–G protein complexes, where a GPCR-homodimer interacts with two Gαβγ-heterotrimers (Fig. 1) [30]. However, in literature, the asymmetric receptor–G protein–model is preferred [26, 30, 41]. These studies suggest, that the $h\beta_2R$ establishes, besides heterodimers, constitutive homodimers, which are expressed at the surface of mammalian cells and furthermore that $h\beta_2R$ dimers play an important role in signal transduction [42]. Some crystal structures with homodimeric GPCRs are available [43–45]. These crystal structures reveal two different GPCR-GPCR contact surfaces: For the ligand-free opsin (3CAP) [43], the κ-opioid receptor (4DJH) [44], and the β_1-adrenergic receptor (4GPO) [46], a GPCR-GPCR contact TM I,VII–TM I,VII was observed, whereas a TM IV, V–TM IV,V contact was found for the chemokine CXCR4 receptor (3OE9) [45]. However, a distinct number of other contact sites should be taken generally into account. It is also discussed that different contact surfaces might be considered and that the contact surfaces might be receptor-specific [47]. Until now, no crystal structure of an active state receptor–G protein–homodimer is known. Thus, the aim of this study is, to use a combined potential-energy-surface-scan/molecular dynamics approach to predict asymmetric and symmetric $h\beta_2R$-Gαβγ-homodimers in order to obtain a more detailed insight into structures of GPCR dimers on molecular level. Furthermore, the main objective was to predict the existence of a symmetric $h\beta_2R$-Gαβγ-homodimer and not the detection of different conformations of this dimer, caused by geometrical changes of the complex using molecular dynamic simulations.

Materials and methods

Crystal structures and homology modeling For modeling of the inactive $h\beta_2R$, the crystal structure of the $h\beta_2R$ (2RH1) [6] and for modeling of the $h\beta_2R$-Gαβγ-complex, the crystal structure of the $h\beta_2R$-Gαβγ-complex (3SN6) [11] were used as template. For homology modeling, the software SYBYL 7.0 (Tripos; http://www.tripos.com/) was used.

- **$h\beta_2R$**: The artificial mutations Glu^{187} (2RH1) and Thr^{96}, Thr^{98} and Glu^{187} (3SN6) in the crystal structures were changed into Asn^{187} (2RH1) and Met^{96}, Met^{98} and Asn^{187} (3SN6) in the models, according to the amino acid sequence (Fig. 2). The amino acids $Ala^{176}Thr^{177}His^{178}$, which are missing in the 3SN6 - crystal structure, were inserted by the loop search module of SYBYL 7.0. Furthermore, the N-terminus and I3-loop, which are missing in the crystal structures, were included in the models: The first 28 (2RH1) or 29 (3SN6) missing amino acids of the N-terminus were added to the receptor models with SYBYL, using a random conformation for the backbone. Afterward, position restraints were set onto the whole inactive $h\beta_2R$ and active $h\beta_2R$-Gαβγ-complex, except the added amino acids of the N-terminus. The structures were energetically minimized using SYBYL. Subsequently, short gas phase MD simulations (500 ps) of the N-terminus with the same position restraints, as used for the minimization, were performed. The resulting models for the inactive $h\beta_2R$ and the active $h\beta_2R$-Gαβγ-complex were used for insertion of the missing I3-loop. The 32 (2RH1) or 25 (3SN6) missing amino acids of the I3-loop were introduced into the receptor models using the loop-search module of SYBYL and 50 search results were obtained for the inactive and active model, each. All results leading to no collision between the inserted amino acids of the I3-loop and the residual part of the models ($h\beta_2R$ and $h\beta_2R$-Gαβγ) were energetically minimized with SYBYL. Therefore, position restraints were set onto the whole $h\beta_2R$ and $h\beta_2R$-Gαβγ-complex, except the inserted amino acids of the I3-loop. After minimization, short gas phase MD simulations (500 ps) of the I3-loop with the same position restraints, as used for minimization, were performed with SYBYL. The structures (one for $h\beta_2R$ and one for $h\beta_2R$-Gαβγ) with lowest energy after the 500 ps simulations were used for further modeling. The C-terminal amino acids Leu^{342} to Leu^{413} are missing in the crystal structures of the $h\beta_2R$ or $h\beta_2R$-Gαβγ-complex [6, 11]. In general, it has to be taken into account, that the C-terminus might play a role in interaction with the G protein. However, a correct predictive modeling of the 72 missing amino acids is not possible. Thus, the amino acids Leu^{342} to Leu^{413} were not included in the models, due to conformational uncertainty. Highly conserved water molecules [48] were included in both models.
- **$G\alpha_s$-subunit**: In the crystal structure, the amino acids Met^{1} to Lys^{8}, Met^{60} to Glu^{87}, Leu^{203}, Thr^{204} and Val^{256} to Gln^{262} are missing. These amino acids were included in the model according to the following procedure: Met^{1} to Lys^{8} were added with a helical structure, continuing the

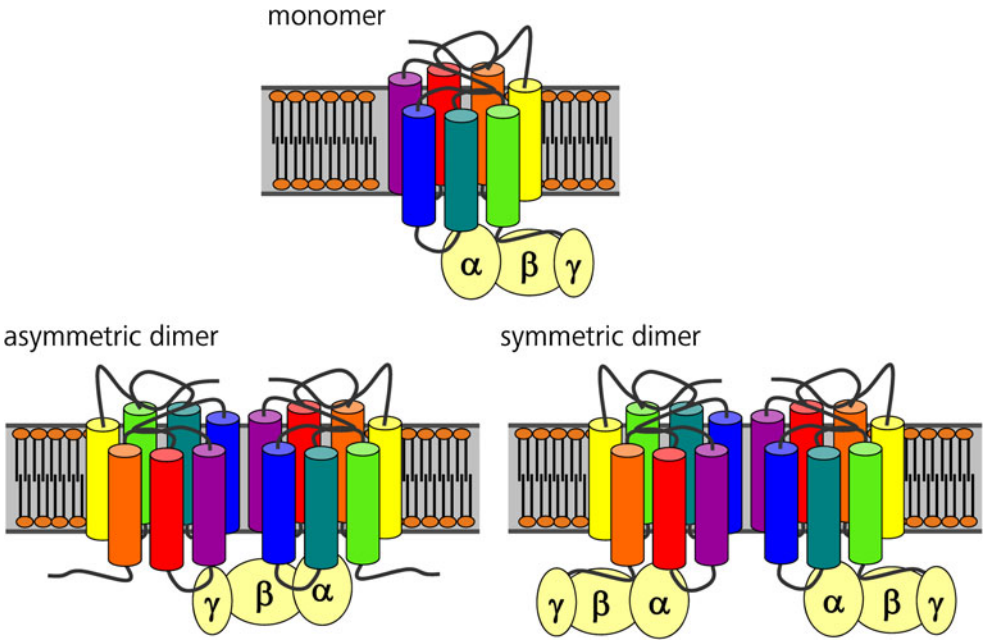

Fig. 1 Schematics of different GPCR-G-protein interaction models. Monomer (one GPCR interacts with one Gαβγ), asymmetric dimer (two GPCRs are in close contact, but only one GPCR interacts with one Gαβγ), symmetric dimer (two GPCRs are in close contact and each GPCR interacts with a Gαβγ)

helix, observed for Thr[9] to Arg[38] in the crystal structure 3SN6. Met[60] to Glu[87] and Val[256] to Gln[262] were adopted according the 1AZT [49]. Leu[203] and Thr[204] were included via the loop-search module of SYBYL 7.0.

hβ_2R

```
    |--------N-Terminus----------||-----------TMI--------------||--I1-|---------TMII---
  1-MGQPGNGSAFLLAPNGSHAPDHDVTQQRDEVWVVGMGIVMSLIVLAIVFGNVLVITAIAKFERLQTVTNYFITSLACADLVMG-83
    ------------||-E1-||------------TMIII--------------||----C2-----||---------TMIV----
 84-LAVVPFGAAHILMKMWTFGNFWCEFWTSLDVLCVTASIETLCVIAVDRYFAITSPFKYQSLLTKNKARVIILMVWIVSGLTSF-166
    ---||-----------E2----------||----------TMV-----------||----------------------C3---
167-LPIQMHWYRATHQEAINCYANETCCDFFTNQAYAIASSIVSFYVPLVIMVFVYSRVFQEAKRQLQKIDKSEGRFHVQNLSQVE-249
    ------------------||------------TMVI-------------||--E3-||--------TMVII-------||-----
250-QDGRTGHGLRRSSKFCLKEHKALKTLGIIMGTFTLCWLPFFIVNIVHVIQDNLIRKEVYILLNWIGYVNSGFNPLIYCRSPDF-332
    ------------------------C-Terminus--------------------------------------------|
333-RIAFQELLCLRRSSLKAYGNGYSSNGNTGEQSGYHVEQEKENKLLCEDLPGTEDFVGHQGTVPSDNIDSPGRNCSTNDSLL-413
```

bGα_s (bos taurus, expasy accession code:P04896)

```
  1-MGCLGNSKTEDQRNEEKAQREANKKIEKQLQKDKQVYRATHRLLLLGAGESGKSTIVKQMRILHVNGFNGEGGEEDPQAARSN-83
 84-SDGEKATKVQDIKNNLKEAIETIVAAMSNLVPPVELANPENQFRVDYILSVMNVPDFDFPPEFYEHAKALWEDEGVRACYERS-166
167-NEYQLIDCAQYFLDKIDVIKQDDYVPSDQDLLRCRVLTSGIFETKFQVDKVNFHMFDVGGQRDERRKWIQCFNDVTAIIFVVA-249
250-SSSYNMVIREDNQTNRLQEALNLFKSIWNNRWLRTISVILFLNKQDLLAEKVLAGKSKIEDYFPEFARYTTPEDATPEPGEDP-332
333-RVTRAKYFIRDEFLRISTASGDGRHYCYPHFTCAVDTENIRRVFNDCRDIIQRMHLRQYELL-394
```

hGβ_1 (rattus norvegicus, expasy accession code: P54311)

```
  1-MSELDQLRQEAEQLKNQIRDARKACADATLSQITNNIDPVGRIQMRTRRTLRGHLAKIYAMHWGTDSRLLVSASQDGKLIIWD-83
 84-SYTTNKVHAIPLRSSWVMTCAYAPSGNYVACGGLDNICSIYNLKTREGNVRVSRELAGHTGYLSCCRFLDDNQIVTSSGDTTC-166
167-ALWDIETGQQTTTFTGHTGDVMSLSLAPDTRLFVSGACDASAKLWDVREGMCRQTFTGHESDINAICFFPNGNAFATGSDDAT-249
250-CRLFDLRADQELMTYSHDNIICGITSVSFSKSGRLLLAGYDDFNCNVWDALKADRAGVLAGHDNRVSCLGVTDDGMAVATGSW-332
333-DSFLKIWN-340
```

hGγ_2 (bos taurus, expasy accession code: P63212)

```
  1-MASNNTASIAQARKLVEQLKMEANIDRIKVSKAAADLMAYCEAHAKEDPLLTPVPASENPFREKKFFCAIL-71
```

Fig. 2 Amino acid sequences of the hβ_2R, Gα, Gβ and Gγ. hβ_2R: *bold*, *gray shaded*: highly conserved amino acids

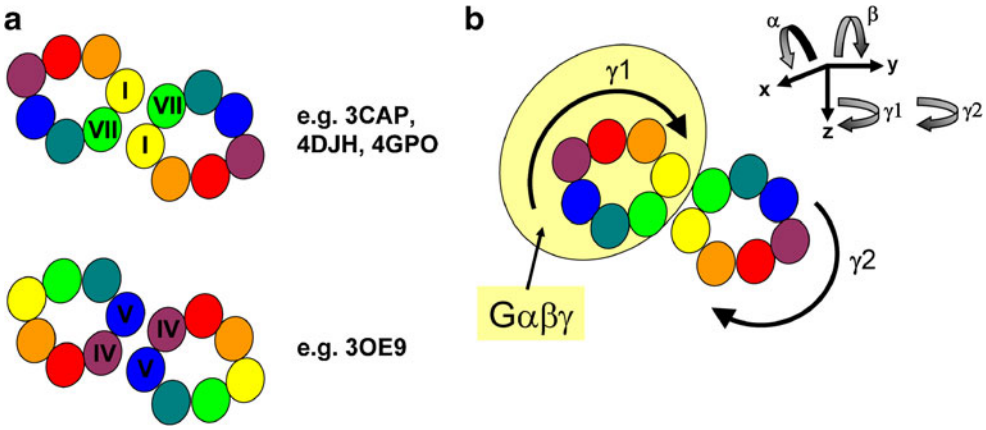

Fig. 3 **a** Schematic presentation of two different GPCR-GPCR interaction models, with the pdb code of the corresponding crystal structures [43–45]. **b** Schematic presentation of a systematic scan with regard to GPCR-GPCR contact sites

– **Gβ_1-subunit**: The artificial Gln^1 in the crystal structure was changed into a Met^1 within the model, according to the amino acid sequence of bovine Gβ_1 (Fig. 2).
– **Gγ_2-subunit**: The amino acids Met^1 to Asn^4 and Glu^{63} to Leu^{71}, missing in the crystal structure, were not included in the model, since they are not important for modeling of dimers.

The artificial Gs-binding nanobody (Nb35) (cocrystallized in 3SN6) and T4 lysozyme (cocrystallized in 2RH1 and 3SN6) were not included in the models. The ligand (P0G) was docked into the active state hβ_2R as indicated by the crystal structure.

Nomenclature For the monomeric and different dimeric hβ_2R-G$\alpha\beta\gamma$-complexes, the following nomenclature is used:

- Monomeric hβ_2R-G$\alpha\beta\gamma$: hβ_2R: r^{mono}; Gα: α^{mono}; Gβ: β^{mono}; Gγ: γ^{mono}
- Asymmetric homodimers hβ_2R-G$\alpha\beta\gamma$-hβ_2R:

– GPCR–G protein complex I: hβ_2R: r1^{asym}; Gα: $\alpha1^{asym}$; Gβ: $\beta1^{asym}$; Gγ: $\gamma1^{asym}$
– GPCR II: hβ_2R: r2^{asym}

- Symmetric homodimer hβ_2R-G$\alpha\beta\gamma$-hβ_2R-G$\alpha\beta\gamma$:

– GPCR–G protein complex I: hβ_2R: r1^{symdim}; Gα: $\alpha1^{symdim}$; Gβ: $\beta1^{symdim}$; Gγ: $\gamma1^{symdim}$
– GPCR–G protein complex II: hβ_2R: r2^{symdim}; Gα: $\alpha2^{symdim}$; Gβ: $\beta2^{symdim}$; Gγ: $\gamma2^{symdim}$

Generation of homodimeric hβ_2R-G$\alpha\beta\gamma$-models The initial structures of the asymmetric and symmetric homodimers were generated with SYBYL by manual docking of the appropriate proteins, paying attention that no collisions between the proteins occur. In order to avoid extensive computational time to identify energetically favored structures of asymmetric and symmetric dimer, first a systematic scan of the potential energy surface was performed, similar, as already described for the interaction between the hβ_2R and the Gα-subunit [23]. Similar studies of potential energy surfaces were performed with regard to agonist pathways to GPCRs [50]. Therefore, the position of the first hβ_2R-G$\alpha\beta\gamma$-complex was fixed, and the second hβ_2R (inactive and active in case of asymmetric dimers) or hβ_2R-G$\alpha\beta\gamma$-complex (in case of symmetric dimers) was systematically translated in x-, y- and z-directions and rotated around the x-, y- and z-axes. Translation along the axes was performed with an increment of 0.15 nm and rotation around the axes was performed with an angle increment of 15°. The contact surface between two hβ_2Rs, was estimated using the "separated surface" command of SYBYL.

Simulation box and molecular dynamic simulations The molecular dynamic simulations were performed with GROMACS 4.0.2 [51]. All models (monomer and symmetric dimer, Fig. 3), including the ligand (P0G), were placed into a POPC lipid bilayer and solvated using a protocol similar to one described in literature [52]: The POPC lipid bilayer (about 13 nm x 13 nm in the xy-plane) was constructed with the software VMD [53] and the hβ_2R-G$\alpha\beta\gamma$-complexes were inserted manually into the membrane, so that the C-terminal part of the hβ_2R was below and parallel to the membrane plane and that the G$\alpha\beta\gamma$-complex was below the lipid bilayer. All lipid molecules colliding with the protein were removed. The resulting systems, consisting of the protein and lipid molecules were solvated with water using the GROMACS utility *genbox*. All water molecules located between the receptor and the aliphatic part of the lipid bilayer were removed. To achieve neutrality, an appropriate number of sodium and chlorine ions were put into the solvation box using the GROMACS utility *genion*. All simulation boxes contained a number of about 400 POPC molecules and about 55,000 to 58,000 water molecules. The size of the simulation boxes was about (13 nm)×(13 nm)×(14.5 nm). For the protein, the ffG53a6 force field [54] was used, whereas the force field parameters for the ligand (P0G) were obtained

from the PRODRG server [55]. For the POPC lipid, the force field parameters available at an appropriate source on the internet (http://moose.bio.ucalgary.ca/index.php?page=Structures_and_Topologies) were used. Parameters for minimization and molecular dynamic simulations are used, as already described [23]. During an equilibration phase of 5 ns, force constants (250 kJ/(mol nm^2) for the first 2.5 ns and 100 kJ/(mol nm^2) for the second 2.5 ns) were put onto the backbone atoms of the transmembrane domains of hβ_2R and onto all backbone atoms of the G$\alpha\beta\gamma$-complex. All force constants were removed during the 20 ns productive phase of MD simulation. The total energy of the simulation boxes and the box volumes are stable during the whole productive simulation phase (Fig. S1). The interior of the POPC-bilayer remained free of water, as exemplary shown for the symmetric homodimer during the whole simulations (Fig. S2) and is in good accordance to data in literature [56]. Interaction energies were calculated using the GROMACS utility *g_energy*.

Results and discussion

Potential energy surface scan of the asymmetric and symmetric homodimeric hβ_2R-G$\alpha\beta\gamma$-complex The potential energy surface scan reveals distinct minima for the asymmetric active hβ_2R-G$\alpha\beta\gamma$–inactive hβ_2R–complex and the active hβ_2R-G$\alpha\beta\gamma$–active hβ_2R–complex (Fig. 4). Two distinct minima can be related with two different dimers: first, a dimer with a TM IV/V-contact and second, a dimer with a TM I/VII-contact (Fig. 4). For both dimers, the helical hβ_2R-hβ_2R-contact is well established. Dimers with analogue contact were already detected in crystal structures (Fig. 3a) [43–46]. Besides, the scan reveals additional minima, e.g., a dimer with the TM V/VI- or TM I/II-contact. But here the helical contact surface of both hβ_2Rs is not as large as for the TM IV/V- or TM I/VII-dimers. However, within GPCR dimers, a helical contact between both GPCRs should be present, but there is little knowledge about the impact of the size of contact surface onto GPCR dimers. In Fig. 4, the regions of the potential energy surface with no contact of TM domains of both hβ_2Rs are presented by the transparency white areas. These data show that for the active hβ_2R-G$\alpha\beta\gamma$–inactive hβ_2R–complex more conformations with helical contact between both hβ_2Rs are present than for the active hβ_2R-G$\alpha\beta\gamma$–active hβ_2R–complex. One reason for this may be the difference in conformation between an inactive and active hβ_2R in the lower part of TM VI [5–7, 11].

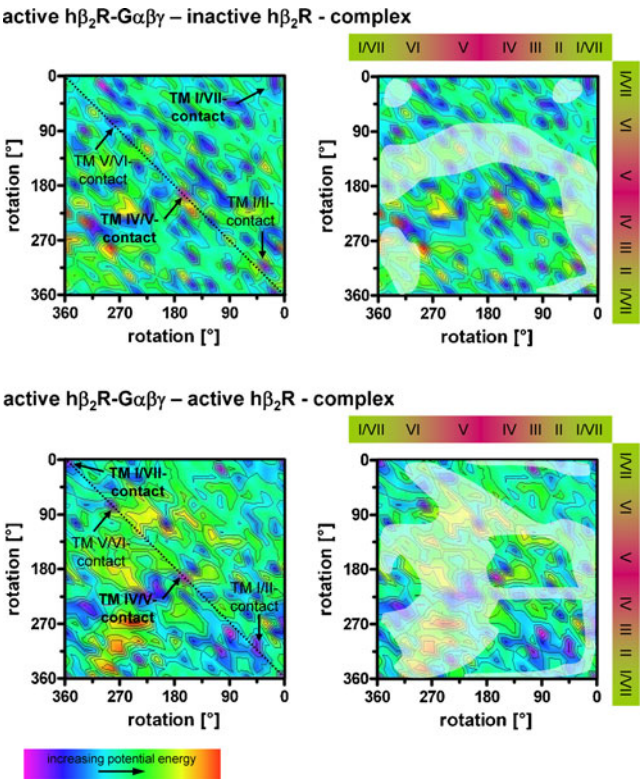

Fig. 4 Results of the potential energy surface scan for the asymmetric active hβ_2R-G$\alpha\beta\gamma$ – inactive hβ_2R-complex and asymmetric active hβ_2R-G$\alpha\beta\gamma$–active hβ_2R-complex. The white shaded areas represent regions with no helical contact between both GPCRs

In general, the potential energy surface scan of the symmetric homodimeric hβ_2R-G$\alpha\beta\gamma$-complex revealed several local minima. A 2D section with regard to rotation of hβ_2R-G$\alpha\beta\gamma$ (I) and hβ_2R-G$\alpha\beta\gamma$ (II) around their individual z-axis (Fig. 3b), provided that an optimal van-der-Waals distance between hβ_2R-G$\alpha\beta\gamma$ (I) and hβ_2R-G$\alpha\beta\gamma$ (II) is obtained, is presented in Fig. 5a. A detailed analysis concerning the hβ_2R-hβ_2R-contact reveals that only one minimum can be related with a structure, in which the TM-domains of both hβ_2Rs are in direct contact via TM I/VII (Fig. 5a). The corresponding structure is assigned as symmetric hβ_2R-G$\alpha\beta\gamma$-dimer. A more detailed presentation regarding the potential energy surface in the region of the hβ_2R-G$\alpha\beta\gamma$-dimer is given in Fig. 5b and c. A translation of the second hβ_2R-G$\alpha\beta\gamma$ (II) in direction to the first hβ_2R-G$\alpha\beta\gamma$ (I) along x- and y-axis without large increase in potential energy is only possible within a very small range (Fig. 5b). This is also true for the rotation of the second hβ_2R-G$\alpha\beta\gamma$ (II) relative to the first hβ_2R-G$\alpha\beta\gamma$ (I) around the x- and y-axis (Fig. 5c)

Interaction between both hβ_2Rs in the symmetric homodimer In general, for the symmetric homodimer, a direct interaction between hydrophilic amino acid side chains of both hβ_2Rs was observed during the MD simulations (Figs. 6, 7 and 8). This hβ_2R-hβ_2R-contact surface is mainly established by the amino acids of TM I and TM VII: Val$^{1.33}$, Gly$^{1.36}$, Ile$^{1.37}$, Ser$^{1.40}$, Leu$^{1.41}$, Leu$^{1.44}$, Phe$^{1.48}$, Leu$^{1.52}$, Arg^{333}, Gln^{337}, Leu^{339}, Leu^{340} and Cys^{341} (Fig. 7). For this

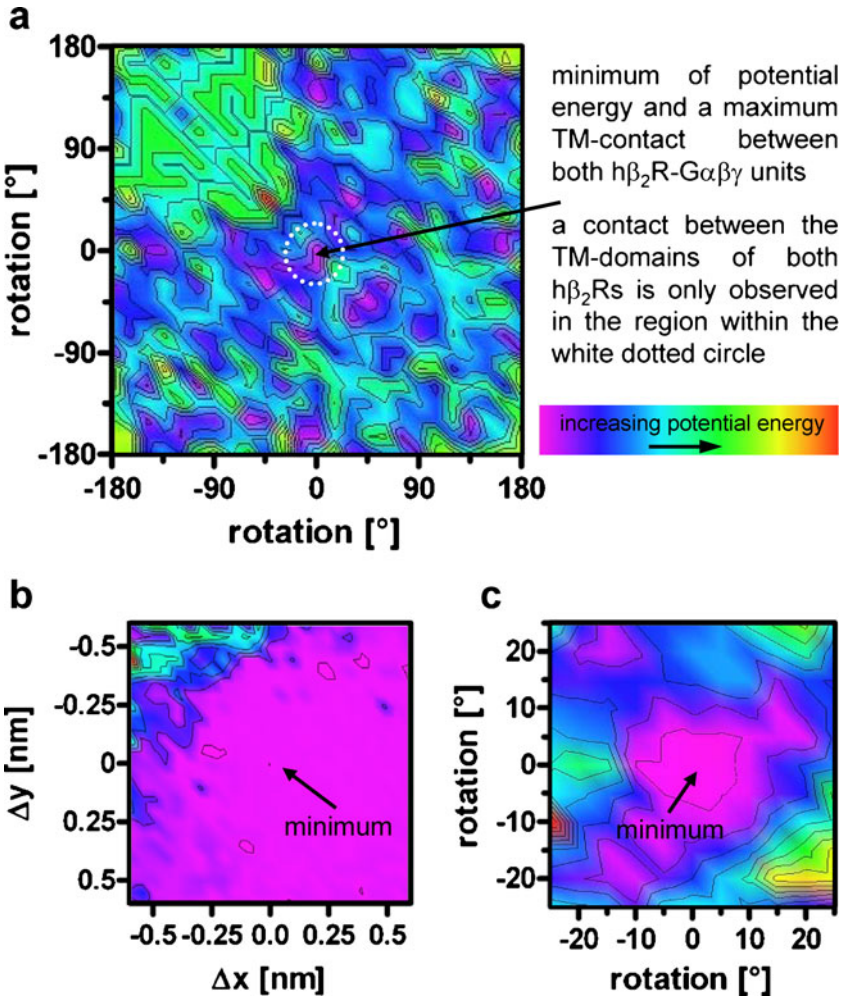

Fig. 5 Results of the potential energy surface scan for the symmetric active hβ$_2$R-Gαβγ-homodimer

interaction mean values of about −363 kJ mol^{-1} were found for the coulombic term and about −366 kJ mol^{-1} for the Lennard-Jones term and showed no significant changes during the simulation (Table 1, Fig. 8). The potential energy of the hβ$_2$R (r^{mono}) in the monomeric complex is slightly increased, compared to the potential energies of both hβ$_2$Rs (r1^{symdim} and r2^{symdim}) in the symmetric homodimer (Fig. 8). This observation might be related to the presence of a second hβ$_2$R-Gαβγ-complex in the symmetric homodimer,

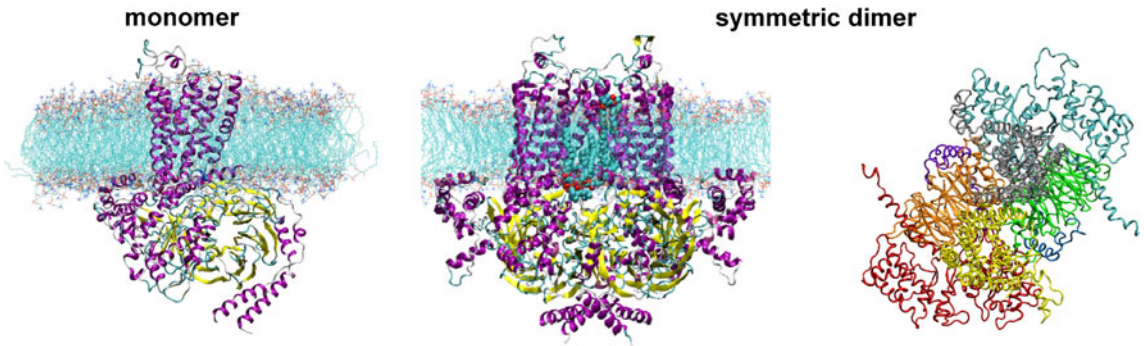

Fig. 6 Structures of the monomeric hβ$_2$R-Gαβγ and the symmetric homodimer. Structures are shown in the lipid bilayer after 10 ns MD simulation in the productive phase. Lipids between both hβ$_2$Rs in the symmetric dimer (*middle*) are shown with a van-der-Waals surface. Color code for symmetric dimer (*right*): hβ$_2$R (r1)–gray, Gα (α1)–cyan, Gβ (β1)–green, Gγ (γ1)–blue; hβ$_2$R (r2)–yellow, Gα (α2)–red, Gβ (β2)–orange, Gγ (γ2)–violet

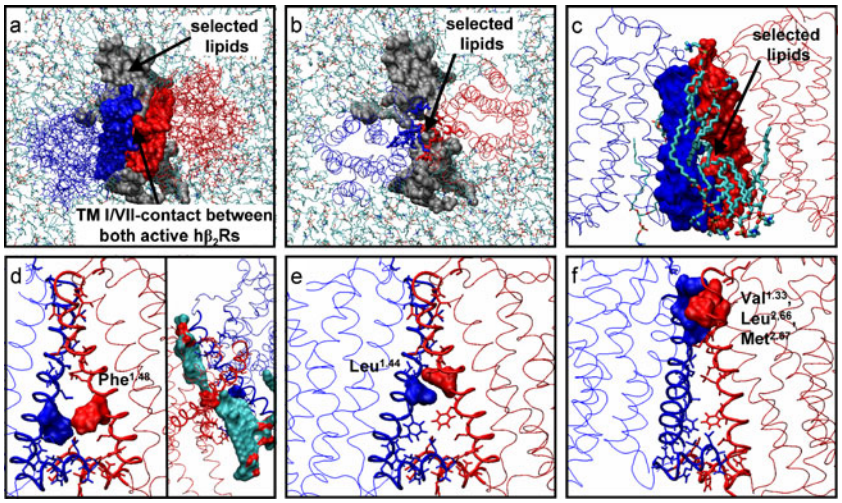

Fig. 7 Interaction between both hβ$_2$Rs in the symmetric homodimer. Coloring: *blue*: hβ$_2$R-Gαβγ-complex I, *red*: hβ$_2$R-Gαβγ-complex II, *gray* surface or cyan sticks: POPC lipids. **a** contact surface (view from the extracellular side) between both hβ$_2$Rs in the symmetric homodimer; the blue and red surfaces are set up by the amino acids of TM I and TM VII; selected POPC lipids, which mediate the interaction between the receptors are given as a *gray* surface. **b** analogue to (**a**), but the amino acids shown as surface (**a**) are now presented as *blue* and *red* sticks. **c** contact surface (view from the side) between both hβ$_2$Rs in the symmetric homodimer; the *blue* and *red* surfaces are set up by the amino acids of TM I and TM VII; selected POPC lipids, which mediate the interaction between the receptors are given as sticks. **d** *left*: contact (view from the side), established by both Phe$^{1.48}$ (presented as surface); *right*: stabilization of this interaction (angular view) by two lipid molecules. **e** contact (view from the side), established by both Leu$^{1.44}$ (presented as surface). **f** contact (view from the side), established by Val$^{1.33}$, Leu$^{2.66}$ and Met$^{2.67}$ (presented as surface) between both hβ$_2$Rs

compared to the monomer. Additionally, the interaction between both GPCRs is mediated by about six lipid molecules (Table 2, Figs. 6 and 7, Fig. S3). Since there is a small gap between both hβ$_2$Rs within the symmetric dimer, in an early phase (≤ 500 ps) of the equilibration, some lipids (≤ 6) penetrated partially into this small gap and remained stable in there (Fig. 7, Fig. S3). Due to the small gap between both hβ$_2$Rs within the symmetric homodimer, the lipid molecules within this gap stabilize the interaction between the hβ$_2$Rs.

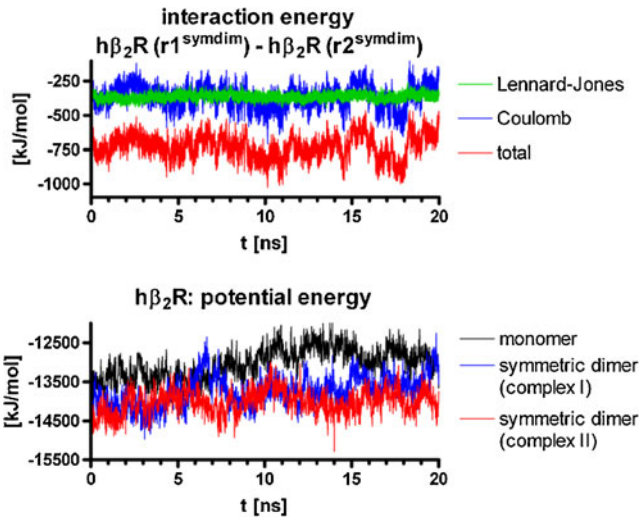

Fig. 8 Time course of the interaction energy between both hβ$_2$Rs in the symmetric dimer and of the potential energy of the hβ$_2$Rs in the monomeric hβ$_2$R-Gαβγ and the symmetric homodimer. The corresponding energies are calculated using the GROMACS utility *g_energy*

Interaction between the Gαβγ-subunits of the symmetric homodimer An interaction energy, different from zero between both Gαβγ-complexes in the symmetric dimer was found between the Gα- and Gβ-subunits, α1-β2 (about −639 kJ mol^{-1}) and α2-β1 (about −497 kJ mol^{-1}), belonging to two different Gαβγ-complexes (Table 1). This interaction is mainly established by electrostatic interactions between Arg^{280}(Gα)-Asp^{267}(Gβ), Arg^{283}(Gα)-Asp^{267}(Gβ), Arg^{347}(Gα)-Asp^{38}(Gβ), Asp^{354}(Gα)-Arg^{42}(Gβ), Arg^{356}(Gα)-Asp^{267}(Gβ) and Arg^{356}(Gα)-Asp^{303}(Gβ). The corresponding mean distances are in a comparable range with respect to the interaction of α1 with β2 and vice versa (Table 3). Differences were only found for two interaction pairs, namely Lys^{274}(Gα)-Asp^{298}(Gβ) and Lys^{274}(Gα)-Asp^{303}(Gβ).

Conformation of the hβ$_2$R in the monomer and the symmetric homodimer For both hβ$_2$Rs in the symmetric hβ$_2$R-Gαβγ-homodimer, large asymmetric conformational changes were observed (Figs. 9, 10 and 11). Within the hβ$_2$R (r1^{symdim}) a movement of the lower part of TM VII toward TM III was

Table 1 Most important interaction energies between the $h\beta_2R$, Gα-, Gβ- and Gγ-subunit of the monomer and symmetric dimer. The interaction energies were calculated with the routine *g_energy*, which is included in GROMACS

		Monomer		Symmetric dimer	
		[kJ mol^{-1}]	∑ [kJ mol^{-1}]	[kJ mol^{-1}]	∑ [kJ mol^{-1}]
α1-β2	$Coul^{SR}$	–	–	−498±74	−639±98
	LJ^{SR}	–		−141±24	
α2-β1	$Coul^{SR}$	–	–	−276±96	−497±118
	LJ^{SR}	–		−221±22	
r1-r2	$Coul^{SR}$	–	–	−363±82	−729±105
	LJ^{SR}	–		−366±23	
r1-α1	$Coul^{SR}$	−970±116	−1455±147	−1417±135	−2088±172
	LJ^{SR}	−485±31		−671±37	
r1-α2	$Coul^{SR}$	–	–	0±0	0±0
	LJ^{SR}	–		0±0	
r2-α1	$Coul^{SR}$	–	–	0±0	0±0
	LJ^{SR}	–		0±0	
r2-α2	$Coul^{SR}$	–	–	−1018±124	−1524±154
	LJ^{SR}	–		−506±30	
r1-P0G1	$Coul^{SR}$	−185±29	−383±41	−203±27	−419±40
	LJ^{SR}	−198±12		−216±13	
r2-P0G2	$Coul^{SR}$	–	–	−156±20	−366±31
	LJ^{SR}	–		−210±11	
r1-β1	$Coul^{SR}$	−353±55	−440±70	−258±62	−321±74
	LJ^{SR}	−87±15		−63±12	
r1-β2	$Coul^{SR}$	–	–	−4±19	−12±26
	LJ^{SR}	–		−8±7	
r2-β2	$Coul^{SR}$	–	–	−195±39	−254±53
	LJ^{SR}	–		−59±14	
r2-β1	$Coul^{SR}$	–	–	0±7	−3±8
	LJ^{SR}	–		−3±1	
α1-β1	$Coul^{SR}$	−1464±140	−2052±187	−1783±166	−2362±206
	LJ^{SR}	−588±47		−579±40	
β1-γ1	$Coul^{SR}$	−1132±106	−1958±143	−1388±125	−2190±163
	LJ^{SR}	−826±37		−802±38	
α2-β2	$Coul^{SR}$	–	–	−1829±136	−2466±182
	LJ^{SR}	–		−637±46	
β2-γ2	$Coul^{SR}$	–	–	−1191±96	−2006±138
	LJ^{SR}	–		−815±42	

observed (Fig. 9, blue curve), as indicated by the distances between the Cα atoms of $Arg^{3.50}$ (100 % conserved within human aminergic GPCRs) and $Tyr^{7.53}$ (94 % conserved within human aminergic GPCRs). Furthermore, the interaction of the highly conserved $Ser^{7.46}$ (94 % conserved within human aminergic GPCRs) and $Asp^{2.50}$ (100 % conserved within human aminergic GPCRs) is lost (Fig. 9, blue curve). Instead, the $Ser^{7.46}$ undergoes a conformational change, thereby shortly establishes a hydrogen bond interaction to the backbone of $Tyr^{7.43}$ (83 % conserved within human amineric GPCRs), and establishes a stable hydrogen bond interaction with the backbone carbon of $Val^{7.44}$ (Fig. 9, blue curve; Fig. 10). Completely different conformational changes were observed for TM VII in the second $h\beta_2R$ ($r2^{symdim}$) of the symmetric dimer (Fig. 9, red curve). Here, the lower part of TM VII moves away from TM III (Fig. 9, red curve) and the interaction between the side chains of $Arg^{3.50}$ and $Tyr^{7.53}$ is broken (Fig. 9, red curve; Fig. 11). Furthermore, the interaction between $Ser^{7.46}$ and $Asp^{2.50}$ remained stable, in contrast to the first $h\beta_2R$ ($r1^{symdim}$), within the first ~17 ns of productive phase (Fig. 9, red curve). An interaction of $Ser^{7.46}$ with $Tyr^{7.43}$ or $Val^{7.44}$, going hand in hand with the loss in interaction between $Ser^{7.46}$ and $Asp^{2.50}$, was observed at about 17 ns (Fig. 9, red curve). Thus, it may be suggested, that the conformational changes observed for both $h\beta_2Rs$ ($r1^{symdim}$ and $r2^{symdim}$) in the

Table 2 Interaction energies between lipid molecules and both hβ_2Rs in the symmetric homodimer. Interaction energies are only shown in case that at least the interaction of the lipid molecule with one hβ_2R is smaller than −50 kJ mol^{-1}. The interaction energies were calculated with the routine *g_energy*, which is included in GROMACS

		r1		r2	
		[kJ mol^{-1}]	∑ [kJ mol^{-1}]	[kJ mol^{-1}]	∑ [kJ mol^{-1}]
POP1	$Coul^{SR}$	−2±6	−65±17	−7±3	−132±17
	LJ^{SR}	−63±11		−125±14	
POP2	$Coul^{SR}$	−124±25	−293±45	−2±1	−71±13
	LJ^{SR}	−169±20		−69±12	
POP3	$Coul^{SR}$	−80±24	−226±42	−199±37	−366±55
	LJ^{SR}	−146±18		−167±18	
POP4	$Coul^{SR}$	−158±26	−305±48	−127±22	−162±35
	LJ^{SR}	−147±22		−35±13	
POP5	$Coul^{SR}$	−301±87	−513±111	0±1	−58±18
	LJ^{SR}	−212±24		−58±17	
POP6	$Coul^{SR}$	−65±18	−144±31	−7±6	−199±41
	LJ^{SR}	−79±13		−192±35	
∑	$Coul^{SR}$	−730±186	−1546±294	−342±70	−988±179
	LJ^{SR}	−816±108		−646±109	

symmetric dimer are related to the presence of the second hβ_2R-G$\alpha\beta\gamma$-unit.

Changes in interaction between the hβ_2R and the Gα-subunit in the monomeric hβ_2R-G$\alpha\beta\gamma$ and symmetric dimer Most important interaction energies for the monomeric hβ_2R-G$\alpha\beta\gamma$-complex and symmetric dimer are summarized in Table 1. For most of these terms, no significant differences between the monomer and symmetric dimer were detected, except for the interaction between hβ_2R and the Gα-subunit: For the monomeric hβ_2R-G$\alpha\beta\gamma$ an interaction energy between hβ_2R (r^{mono}) and Gα (α^{mono}) of about −1455 kJ mol^{-1} was found. This interaction is slightly decreased during the productive phase of simulation (Fig. 12). In contrast, for the symmetric homodimer, an interaction energy of about −2088 kJ mol^{-1} ($r1^{symdim}$-$\alpha1^{symdim}$) and −1524 kJ mol^{-1} ($r2^{symdim}$-$\alpha2^{symdim}$) was observed: Between hβ_2R ($r1^{symdim}$) and Gα ($\alpha1^{symdim}$) the coulomb interaction decreased at about 4 ns to 5 ns and increased again at about 6 ns (Fig. 12). The increase at 6 ns may be related with the decrease in the distance between Arg^{333} (hβ_2R ($r1^{symdim}$)) and Glu^{392} (Gα ($\alpha1^{symdim}$)) (Figs. 9 and 12). Between hβ_2R ($r2^{symdim}$) and Gα ($\alpha2^{symdim}$) the coulomb interaction continuously decreased during the productive phase. Interestingly, the interaction energies between the hβ_2R and Gα changed in the symmetric dimer in an asymmetric manner, which is in good agreement to the observed asymmetric structural changes in both hβ_2Rs.

For the symmetric dimer, a large change in interaction between $Arg^{7.55}$ (hβ_2R) or Arg^{333} (hβ_2R) with Glu^{392} was observed (Figs. 9 and 11). For the first hβ_2R ($r1^{symdim}$) the distance between $Arg^{7.55}$ (hβ_2R, $r1^{symdim}$) and Glu^{392} (Gα, $\alpha1^{symdim}$) remains stable at about 0.4 nm during the productive phase, whereas the distance between Arg^{333} (hβ_2R,

Table 3 Electrostatic interactions between the Gα- and Gβ-subunits in the symmetric homodimer. Distances between positively charged (arginine, lysine) and negatively charged amino acids (aspartate, glutamate) at the contact surface between the Gα- and Gβ-subunits of different G$\alpha\beta\gamma$-complexes. Distances are only shown, if the mean distance is smaller than 1 nm for at least one pair, $\alpha1$-$\beta2$ or $\alpha2$-$\beta1$

Amino acid of the Gα-subunit	Amino acid of the Gβ-subunit	Reference atoms for distance	α1-β2 distance [nm]	α2-β1 distance[nm]
Lys^{274}	Asp^{298}	NZ-CG	1.19±0.07	0.80±0.05
Lys^{274}	Asp^{303}	NZ-CG	1.14±0.13	0.63±0.09
Arg^{280}	Asp^{267}	CZ-CG	0.68±0.09	0.81±0.09
Arg^{283}	Asp^{267}	CZ-CG	0.72±0.15	0.46±0.06
Arg^{347}	Asp^{38}	CZ-CG	0.90±0.14	0.90±0.26
Asp^{354}	Arg^{42}	CG-CZ	0.82±0.16	0.55±0.14
Arg^{356}	Asp^{267}	CZ-CG	0.95±0.18	0.97±0.18
Arg^{356}	Asp^{303}	CZ-CG	1.03±0.25	1.09±0.22

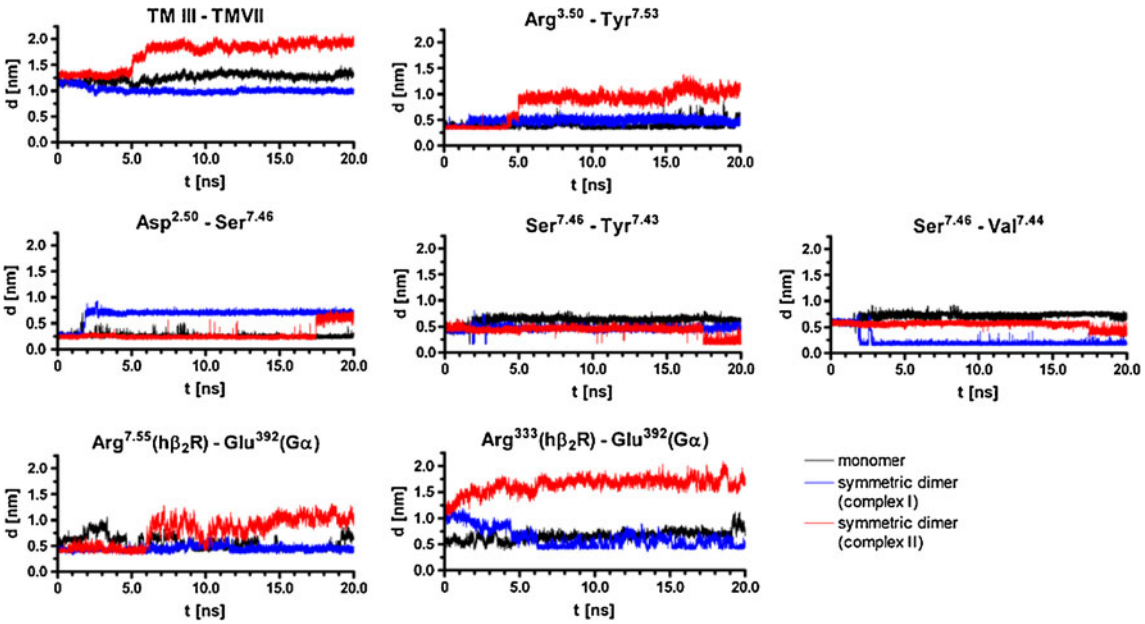

Fig. 9 Time course of distinct structural changes in the monomeric and symmetric dimer during 20 ns productive molecular dynamic simulation. Reference atoms for determination of distances: TM III – TM VII: TM III: Cα-atom of $Arg^{3.50}$, TM VII: Cα-atom of $Tyr^{7.53}$; $Arg^{3.50}$-$Tyr^{7.53}$: $Arg^{3.50}$, CZ (carbon atom of the guanidine moiety), $Tyr^{7.53}$, O (oxygen of the hydroxy group); $Asp^{2.50}$-$Ser^{7.46}$: $Asp^{2.50}$, CG (carbon of the carboxy moiety), $Ser^{7.46}$, HG (hydrogen of the hydroxyl group); $Ser^{7.46}$-$Tyr^{7.43}$: $Ser^{7.46}$, HG (hydrogen of the hydroxyl group), $Tyr^{7.43}$, O (carbonyl oxygen of the backbone); $Ser^{7.46}$-$Val^{7.44}$: $Ser^{7.46}$, HG (hydrogen of the hydroxyl group), $Val^{7.44}$, O (carbonyl of the backbone); $Arg^{7.55}(h\beta_2R)$-$Glu^{392}(G\alpha)$: $Arg^{7.55}$, CZ (carbon atom of the guanidine moiety), Glu^{392}, CD (carbon of the carboxy moiety); $Arg^{333}(h\beta_2R)$-$Glu^{392}(G\alpha)$: Arg^{333}, CZ (carbon atom of the guanidine moiety), Glu^{392}, CD (carbon of the carboxy moiety)

$r1^{symdim}$) and Glu^{392} (Gα, $\alpha1^{symdim}$) decreases in two steps from about 1.0 nm to 0.4 nm. In contrast, for the second $h\beta_2R$ ($r2^{symdim}$), the distance between $Arg^{7.55}$ ($h\beta_2R$, $r2^{symdim}$) and Glu^{392} (Gα, $\alpha2^{symdim}$) on the one hand and between Arg^{333} ($h\beta_2R$, $r2^{symdim}$) and Glu^{392} (Gα, $\alpha2^{symdim}$) on the other hand increases (Figs. 9 and 11).

Interaction between the ligand and $h\beta_2R$ In general, distinct hydrogen bond interactions between the ligand (P0G) and the $h\beta_2R$ were observed within the simulation of the monomeric $h\beta_2R$-Gαβγ- and the symmetric homodimeric $h\beta_2R$-Gαβγ-$h\beta_2R$-Gαβγ-complex, with $Asp^{3.32}$, $Thr^{5.34}$, $Ser^{5.42}$, $Ser^{5.46}$, $Tyr^{7.35}$, $Asn^{7.39}$, and $Tyr^{7.43}$ being involved (Fig. S4). Within the monomeric $h\beta_2R$-Gαβγ-complex, the ligand established direct hydrogen bonds to these amino acids, except $Tyr^{7.35}$. In contrast, a direct H-bond interaction between the ligand and $Tyr^{7.35}$ was observed within both $h\beta_2Rs$ of the symmetric homodimer. Differences between the direct ligand-receptor interaction within the monomer or symmetric homodimer were also observed concerning $Thr^{5.34}$, $Ser^{5.42}$ and $Ser^{5.46}$ (Fig. S4). Additionally, water molecules, which are present in the binding pocket, were observed to mediate the interaction between the ligand P0G and the $h\beta_2R$ for the monomer and symmetric homodimer (Fig. S4). However, the overall orientation of the ligand in the binding pocket of the $h\beta_2Rs$ in the monomer and symmetric dimer did not change during the simulations. Thus, large differences in the binding mode of P0G within the $h\beta_2R$ of the monomer and symmetric dimer were not observed.

Summarized comparison of the analyzed monomer and symmetric homodimer Within this study, distinct asymmetric and one symmetric $h\beta_2R$-Gαβγ-homodimers were identified by a potential energy surface scan. In literature, some simulation data, addressing GPCR dimers are available [28, 33, 34, 36]. However, some of these studies did not include the Gαβγ-complex [28, 33, 36]. This may lead to wrong predictions of homo- or heterodimeric GPCR models, because in presence of one or two Gαβγ-complexes, not all configurations of GPCR-GPCR dimers are allowed, because of steric hindrance, compared to the case, where no Gαβγ-complex is present.

Considerable structural differences with respect to the monomeric $h\beta_2R$-Gαβγ-complex were found in the MD

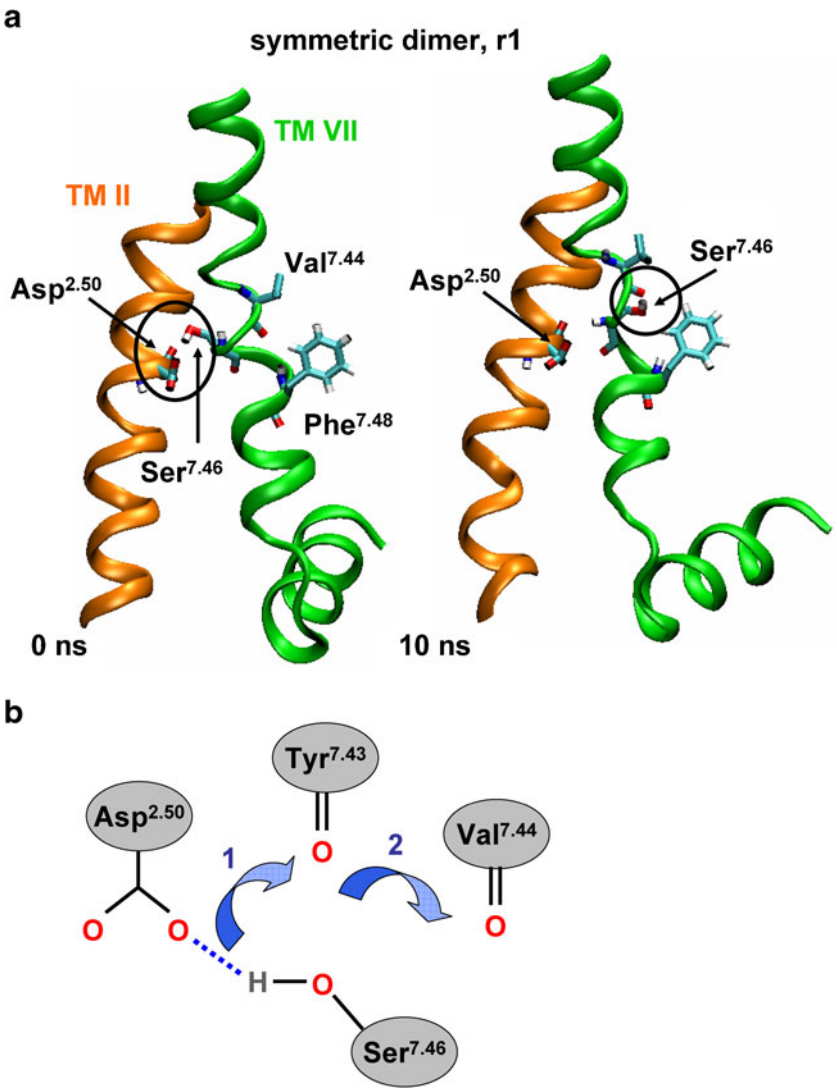

Fig. 10 Structural changes within the $h\beta_2R$ (r1) of the symmetric dimer. **a** Snapshots at the beginning and end of the productive phase of MD simulation. **b** Schematic presentation of the $Ser^{7.46}$-switch. First, the side chain of $Ser^{7.46}$ establishes an interaction to the carboxy moiety of $Asp^{2.50}$. After structural changes, the side chain of $Ser^{7.46}$ interacts with the backbone carbonyl of $Tyr^{7.53}$ and after further structural changes, the side chain of $Ser^{7.46}$ interacts with the backbone carbonyl of $Val^{7.44}$. The structural changes, presented in this scheme were only observed for some distinct dimers, as described in "Results and discussion"

simulation of the symmetric dimer. A remarkable conformational change was observed in the lower part of TM VII. For one $h\beta_2R$, the interaction between $Arg^{3.50}$ and $Tyr^{7.53}$ was lost. Subsequently, TM VII was straightened and the electrostatic interaction between $Arg^{7.55}$ or Arg^{333} and Glu^{392} of the C-terminal part of the Gα-subunit decreased due to an increasing distance between the arginine and glutamate side chains. For the second $h\beta_2R$ in the symmetric dimer contrary structural changes were observed. Here, the lower part of TM VII moved in direction of TM III and the electrostatic interaction between the $h\beta_2R$ ($Arg^{7.55}$, Arg^{333}) and the C-terminal part of Gα (Glu^{392}) remained intact. Thus, asymmetric conformational changes were observed for the symmetric homodimer. A pharmacological interpretation of these simulation results is hardly possible, without further theoretical and experimental studies.

Based on the results of the potential energy surface scans (Figs. 4 and 5), it may be speculated about the structure of tetrameric GPCR-complexes. In Fig. 13, two schematic models for those complexes are presented. The symmetric homodimer, described within this study, is localized in the center of the tetramer in both models. On both sides, one inactive $h\beta_2R$ is in close contact to the active $h\beta_2Rs$. In model I, the contact surface between the inactive and active $h\beta_2Rs$ is established by TM IV and V (Fig. 13). This is in accordance to findings in a crystal structure [45] or to the results of the potential energy surface scan (Fig. 4). In contrast, in model II, the

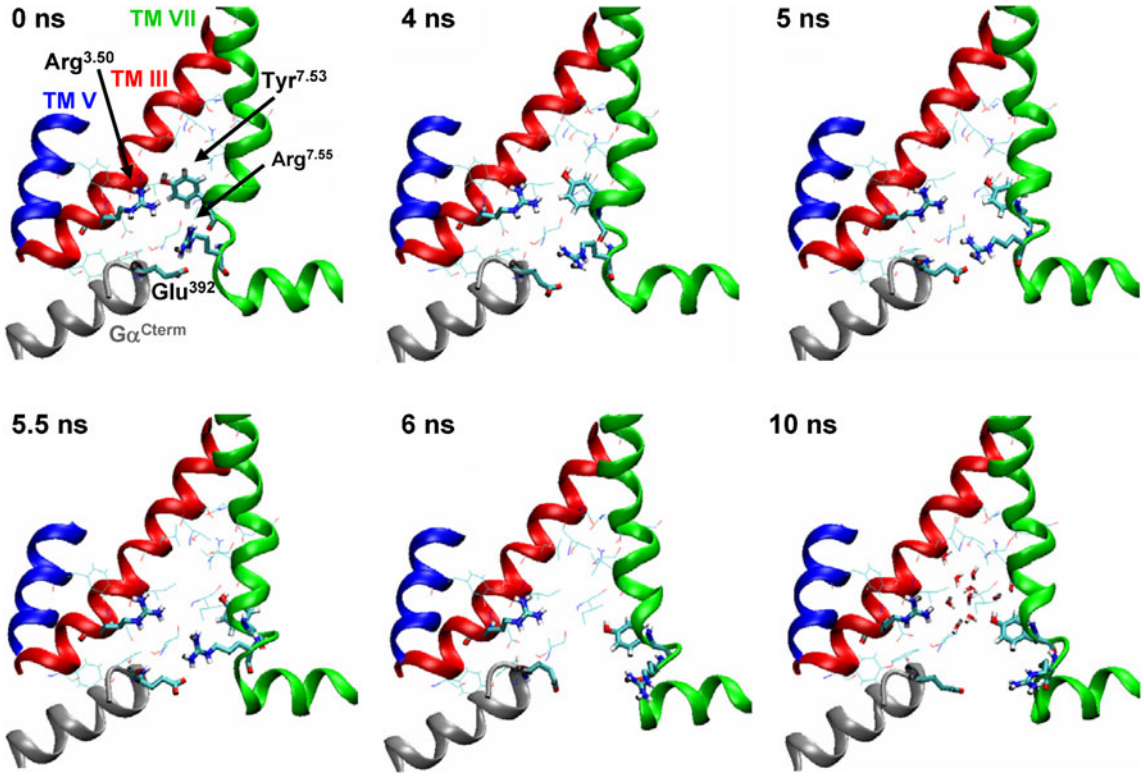

Fig. 11 Snapshots of the hβ_2R (r2) and the C-terminal part of the Gα-subunit (α2) of the symmetric dimer. Snapshots are from the productive phase of MD simulation

contact surface between the inactive and active hβ_2Rs is established by TM V and TM VI (Fig. 13). Such a contact was identified in the potential energy surface scan (Fig. 4) as a local minimum. Both models differ to a model of an oligomeric GPCR complex described in literature [29]. Model I is inverse to an oligomeric complex described with regard to the β_1-adrenergic receptor [46]. In contrast to model I (Fig. 13) the authors describe a tetramer with two inactive

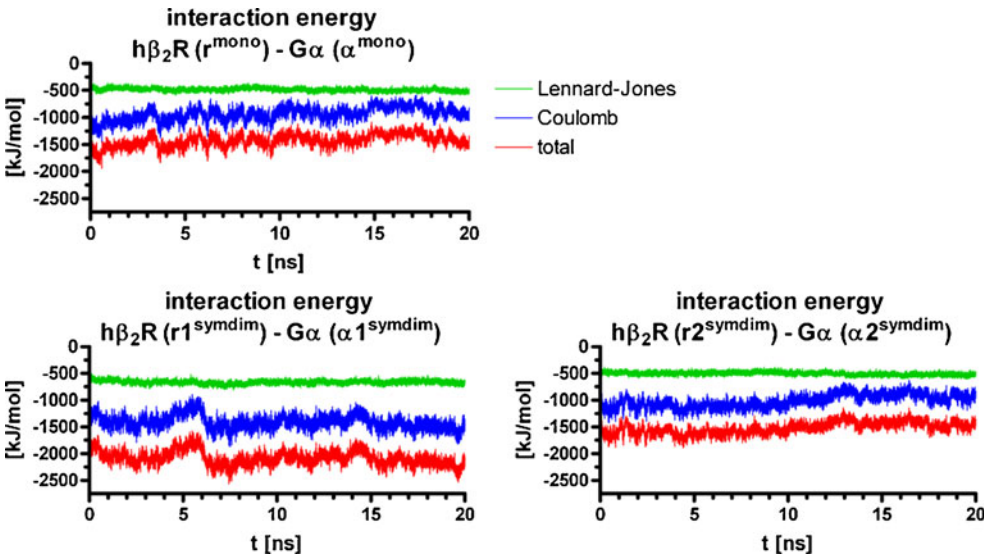

Fig. 12 Time course of the interaction energy between the hβ_2R and the Gα-subunit for the monomeric hβ_2R-Gαβγ and the symmetric homodimer. The corresponding energies are calculated using the GROMACS utility *g_energy*

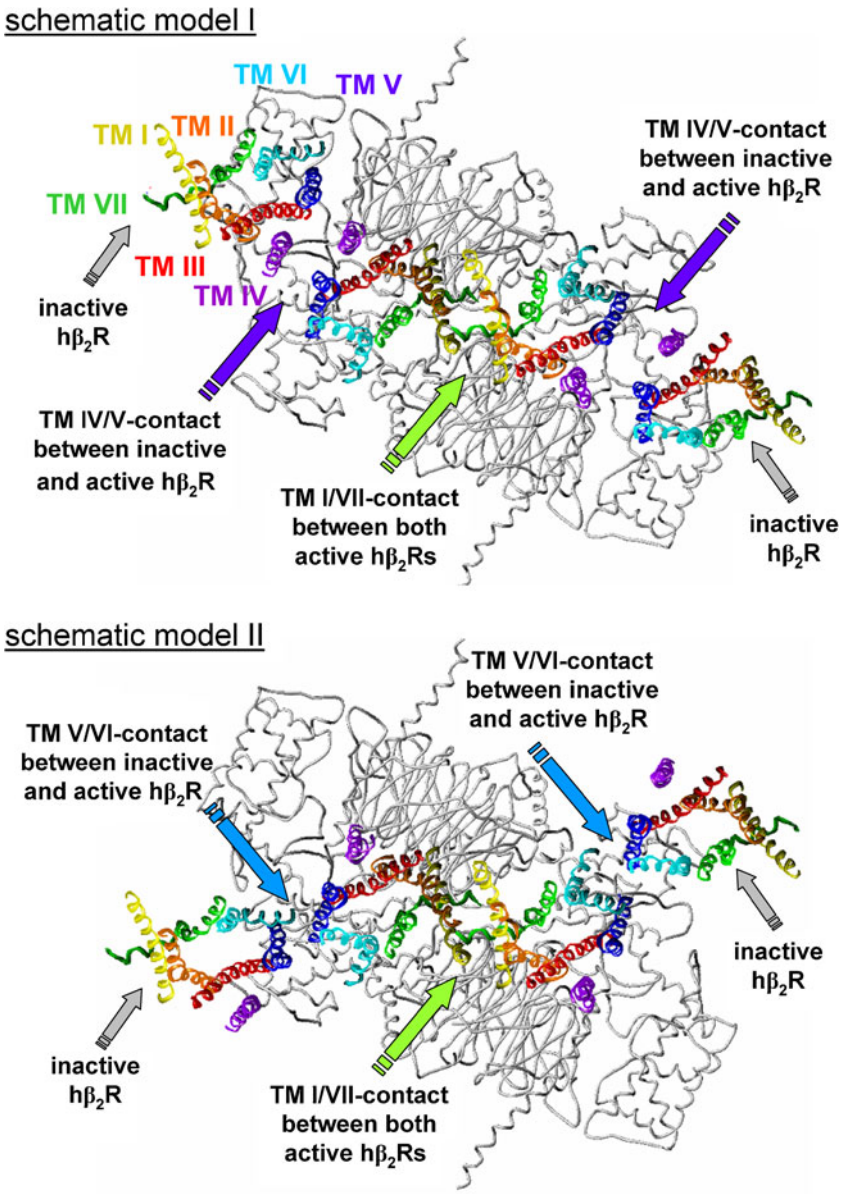

Fig. 13 Schematic models of possible structures for GPCR tetramers. Both models are constructed based on the results of the energy surface scans. Energetic calculations were not performed explicitly for the tetrameric models. The *gray* tubes represent both Gαβγ-complexes

GPCRs located in the center of the complex, whereas the two active GPCR-G-protein-complexes are located at both sides of the inactive dimer [46]. However, both models–the model of Huang and model I (Fig. 13)–are in good accordance with pharmacological results, indicating a 2:1 ratio of GPCR : G-protein [26, 30, 41].

Furthermore, this study shows that the conformation of the Gα-subunit may play an important role concerning some specific contact surfaces of GPCR dimers. So, the TM I,VII–TM I,VII contact surface between two GPCRs can be established, independently of the conformation of the Gα-subunit, but in contrast, for the TM IV,V–TM IV,V contact surface, the conformation of the Gα-subunit, especially the amino acids 48 to 210, plays an important role [11, 49]. If the amino acids 48 to 210 of the Gα-subunit exhibit a conformation, as observed in the 3SN6 crystal, the GPCR-GPCR contact between TM IV,V–TM IV,V can only be established, if the Gα-subunit slightly changes its conformation. In literature, pharmacological data are mainly interpreted based on asymmetric GPCR dimers, whereas only few studies also take into account symmetric dimers [27, 30].

Conclusion

Within this study, we showed that active state symmetric homodimers can be established and so have to be taken into account in order to interpret pharmacological data. Furthermore, our study gives hint to important amino acids, responsible for stabilization of such symmetric homodimers. Based on these data, site-directed mutagenesis studies, combined with pharmacological studies can be performed in order to obtain a more detailed insight into symmetric GPCR dimers on molecular level.

Acknowledgments This work was supported by DFG (STR 1125/1-1) of the Deutsche Forschungsgemeinschaft.

References

1. Foord SM, Bonner TI, Neubig RR, Rosser EM, Pin JP, Davenport AP et al (2005) International union of pharmacology. XLVI. G protein-coupled receptor list. Pharmacol Rev 57:279–299
2. Deupi X, Kobilka BK (2010) Energy landscapes as a tool to integrate GPCR structure, dynamics, and function. Physiology 25:293–303
3. Nygaard R, Zou Y, Dror RO, Mildorf TJ, Arlow DH, Manglik A, Pan AC, Liu CW, Fung JJ, Bokoch MP, Thian FS, Kobilka TS, Shaw DE, Mueller L, Prosser RS, Kobilka BK (2013) The dynamic process of β_2-adrenergic receptor activation. Cell 152:532–542
4. Zocher M, Fung JJ, Kobilka BK, Müller DJ (2012) Ligand-specific interactions modulate kinetic, energetic, and mechanical properties of human β_2 adrenergic receptor. Structure 20:1391–1402
5. Rasmussen SGF, Choi HJ, Rosenbaum DM, Kobilka TS, Thian FS, Edwards PC, Burghammer M, Ratnala VRP, Sanishvili R, Fischetti RF, Schertler GFX, Weis WI, Kobilka BK (2007) Crystal structure of the human β_2 adrenergic G-protein-coupled receptor. Nature 450:383–387
6. Cherezov V, Rosenbaum DM, Hanson MA, Rasmussen SGF, Thian FS, Kobilka TS, Choi HJ, Kuhn P, Weis WI, Kobilka BK, Stevens RC (2007) High-resolution crystal structure of an engineered human β_2-adrenergic G protein-coupled receptor. Science 318:1258–1265
7. Rosenbaum DM, Cherezov V, Hanson MA, Rasmussen SGF, Thian FS, Kobilka TS, Choi HJ, Yao XJ, Weis WI, Stevens RC, Kobilka BK (2007) GPCR engineering yields high-resolution structural insights into β_2-adrenergic receptor function. Science 318:1266–1273
8. Hanson MA, Cherezov V, Griffith MT, Roth CB, Jaakola VP, Chien YET, Velasquez J, Kuhn P, Stevens RC (2008) A specific cholesterol binding site is established by the 2.8 Å structure of the human β_2-adrenergic receptor. Structure 16:897–905
9. Wacker D, Genalti G, Brown MA, Katritch V, Abagyan R, Cherezov V, Stevens RC (2010) Conserved binding mode of the human 2 adrenergic receptor inverse agonists and antagonist revealed by X-ray crystallography. J Am Chem Soc 132:11443–11445
10. Bokoch MP, Zou Y, Rasmussen SGF, Liu CW, Nygaard R, Rosenbaum DM, Fund JJ, Choi HJ, Thian FS, Kobilka TS, Publisi JD, Weis WI, Pardo L, Prosser RS, Mueller L, Kobilka BK (2010) Ligand-specific regulation of the extracellular surface of a G-protein-coupled receptor. Nature 463:108–112
11. Rasmussen SGF, DeVree BT, Zou Y, Kruse AC, Chung KY, Kobilka TS, Thian FS, Chae PS, Pardon E, Calinski D, Mathiesen JM, Shah STY, Lyons JA, Caffrey M, Gellman SH, Steyaert J, Skiniotis G, Weis WI, Sunahara RK, Kobilka BK (2011) Crystal structure of the β_2 adrenergic receptor—Gs protein complex. Nature 477:549–555
12. Oldham WM, Hamm HW (2006) Structural basis of function in heterotrimeric G proteins. Q Rev Biophys 39:117–166
13. Oldham WM, Hamm HE (2008) Heterotrimeric G protein activation by G-protein-coupled receptors. Nat Rev Mol Cell Biol 9:60–71
14. Herrmann R, Heck M, Henklein P, Henklein P, Kleuss C, Hofmann KP, Ernst OP (2004) Sequence of interactions in receptor-G protein coupling. J Biol Chem 279:24283–24290
15. Taylor JM, Jacob-Mosier GG, Lawton RG, Remmers AE, Neubig RR (1994) Binding of an α2 adrenergic receptor third intracellular loop peptide to Gβ and the amino terminus of Gα. J Biol Chem 269:27618–27624
16. Lichtarge O, Bourne HR, Cohen FE (1996) Evolutionarily conserved G$\alpha\beta\gamma$ binding surfaces support a model of the G protein-receptor complex. Proc Natl Acad Sci USA 93:7507–7511
17. Bae H, Cabrera-Vera TM, Depree KM, Graber SG, Hamm HE (1999) Two amino acids within the α4 helix of G_{i1} mediate coupling with 5-hydroxytryptamine$_{1B}$ receptors. J Biol Chem 274:14963–14971
18. Ho MK, Wong YH (2000) The amino terminus of Gαt is required for receptor recognition, whereas the α4/β6 loop is essential for inhibition of adenylyl cyclase. Mol Pharmacol 58:993–1000
19. Greasley PJ, Fanelli F, Scheer A, Abuin L, Nenniger-Tosato M, de Benedetti PG, Cotecchia S (2001) Mutational and computational analysis of the α_{1B}-adrenergic receptor: involvement of basic and hydrophobic residues in receptor activation and G protein coupling. J Biol Chem 276:46485–46494
20. Oliveira L, Paiva PB, Paiva ACM, Vriend G (2003) Sequence analysis reveals how G protein-coupled receptors transduce the signal to the G protein. Proteins 52:553–560
21. Janz JM, Farrens DL (2004) Rhodopsin activation expose a key hydrophobic binding site for the transducin α-subunit C terminus. J Biol Chem 279:29767–29773
22. Raimondi F, Seeber M, de Benedetti PG, Fanelli F (2008) Mechanisms of the inter- and intramolecular communication in GPCRs and G proteins. J Am Chem Soc 130:4310–4325
23. Strasser A, Wittmann HJ (2010) Distinct interactions between the human adrenergic β_2 receptor and Gα_s—an in silico study. J Mol Model 16:1307–1318
24. Strasser A, Wittmann HJ (2012) hβ_2R-Gα_s complex: prediction versus crystal structure—how valuable are predictions based on molecular modelling studies? J Mol Model 18:3439–3444
25. Milligan G (2004) G Protein-coupled receptor dimerization: function and ligand pharmacology. Mol Pharmacol 66:1–7
26. Whorton MR, Bokoch MP, Rasmussen SGF, Huang B, Zare RN, Kobilka, Sunahara RK (2007) A monomeric G protein-coupled receptor isolated in a high-density lipoprotein particle efficiently activates its G protein. PNAS 104:7682–7687
27. Rovira X, Pin JP, Giraldo J (2010) The asymmetric/symmetric activation of GPCR dimers as a possible mechanistic rationale for multiple signalling pathways. Trends Pharmacol Sci 31:15–21
28. Simpson LM, Taddese B, Wall ID, Reynolds CA (2010) Bioinformatics and molecular modelling approachs to GPCR oligomerization. Curr Opin Pharmacol 10:30–37
29. Han Y, Moreira IS, Urizar E, Weinstein H, Javitch JA (2009) Allosteric communication between protomers of dopamine class A GPCR dimers modulates activation. Nat Chem Biol 5:688–695
30. Kamal M, Maurice P, Jockers R (2011) Expanding the concept of G protein-coupled receptor (GPCR) dimer asymmetry toward GPCR-interacting proteins. Pharmaceuticals 4:273–284
31. Fotiadis D, Jastrzebska B, Philippsen A, Müller DJ, Palczewski K, Engel A (2006) Structure of the rhodopsin dimer: a working model for G-protein-coupled receptors. Curr Opin Struc Biol 16:252–259
32. Granier S, Kobilka BK (2012) A new era of GPCR structural and chemical biology. Nat Chem Biol 8:670–673

33. Gorinski N, Kowalsman N, Renner U, Wirth A, Reinartz MT, Seifert R, Zeug A, Ponimaskin E, Niv MY (2012) Computational and experimental analysis of the transmembrane domain 4/5 dimerization interface of the serotonin 5-HT_{1A} receptor. Mol Pharmacol 82:448–463
34. Filizola M (2012) Assessing the relative stability of dimer interfaces in G protein-coupled receptors. PLOS Comput Biol doi: 10.1371/journal.pcbi.1002649
35. Shan J, Khelashvili G, Mondal S, Mehler EL, Weinstein H (2012) Ligand-dependent conformations and dynamics of the serotonin 5-HT_{2A} receptor determine its activation and membrane-driven oligomerization properties. PLOS Comp Biol 8:1–15
36. Periole X, Knepp AM, Sakmar TP, Marrink SJ, Huber T (2012) Structural determinants of the supramolecular organization of G protein-coupled receptors in bilayers. J Am Chem Soc 134:10959–10965
37. Granier S, Manglik A, Kruse AC, Kobilka TS, Thian FS, Weis WI, Kobilka BK (2012) Structure of the δ-opioid receptor bound to naltrindole. Nature 485:400–405
38. Hu J, Thor D, Zhou Y, Liu T, Wang Y, McMillin SM, Mistry R, Challiss RAJ, Costanzi S, Wess J (2012) Structural aspects of M3 muscarinic acetylcholine receptor dimer formation and activation. FASEB J 26:604–616
39. Manglik A, Kruse A, Kobilka TS, Thian TS, Mathiesen JM, Sunahara RK, Pardo L, Weis WI, Kobilka BK, Granier S (2012) Crystal structure of the m-opioid receptor bound to a morphinan antagonist. Nature 485:321–327
40. Katritch V, Cherezov V, Stevens RC (2013) Structure-function of the G protein-coupled receptor superfamily. Annu Rev Pharmacol Toxicol 53:531–556
41. Jastrzebska B, Orban T, Golczak M, Engel A, Palczewski K (2013) Asymmetry of the rhodopsin dimer in complex with transducin. FASEB J 27 doi:10.1096/fj.12-225383
42. Angers S, Salahpour A, Joly E, Hilairet S, Chelsky D, Dennis M, Bouvier M (2000) Detection of beta 2-adrenergic receptor dimerizaion in living cells using bioluminescence resonance energy transfer (BRET). Proc Natl Acad Sci USA 97:3684–3689
43. Park JH, Scheerer P, Hofmann KP, Choe HW, Ernst OP (2008) Crystal structure of the ligand-free G-protein-coupled receptor opsin. Nature 454:183–187
44. Wu H, Wacker D, Mileni M, Katritch V, Han GW, Vardy E, Liu W, Thompson AA, Huang XP, Carroll FI, Mascarella SW, Westkaemper RB, Mosier PD, Roth BL, Cherezov V, Stevens RC (2012) Structure of the human κ-opioid receptor in complex with IDTic. Nature 485:327–332
45. Wu B, Chien EY, Mol CD, Fenalti G, Liu W, Katritch V, Abagyan R, Brooun A, Wells P, Bi FC, Hamel DC, Kuhn P, Handel TM, Cherezov V, Stevens RC (2010) Structures of the CXCR4 chemokine GPCR with small-molecule and cyclic peptide antagonists. Science 330:1066–1071
46. Huang J, Chen S, Zhang J, Huang XY (2013) Crystal structure of oligomeric β1-adrenergic G protein-coupled receptors in ligand-free basal state. Nat Struct Mol Biol 20:419–425
47. Salahpour A, Angers S, Mercier JF, Lagace M, Marullo S, Bouvier M (2004) Homodimerization of the beta-2-adrenergic receptor as a prerequisite for cell surface targeting. J Biol Chem 279:33390–333397
48. Liu W, Chun E, Thompson AA, Chubukov P, Xu F, Katritch V, Han GW, Roth CB, Heitman LH, Ijzerman AP, Cherezov V, Stevens RC (2012) Structural basis for allosteric regulation of GPCRs by sodium ions. Science 337:232–235
49. Sunahara RK, Tesmer JJ, Gilman AG, Sprang SR (1997) Crystal structure of the adenylyl cyclase activator Gsα. Science 278:1943–1947
50. Bhattacharya S, Vaidehi N (2010) Computational mapping of the conformational transitions in agonist selective pathways of a G-protein coupled receptor. J Am Chem Soc 132:5205–5214
51. Van der Spoel D, Lindahl E, Hess B, Groenhof G, Mark AE, Berendsen HFC (2005) GROMACS: fast, flexible, and free. J Comput Chem 26:1701–1718
52. Goetz A, Lanig H, Gmeiner P, Clark T (2011) Molecular dynamics simulations of the effect of the G-Protein and diffusible ligands on the 2-adrenergic receptor. J Mol Biol 414:611–623
53. Humphrey W, Dalke A, Schulten K (1996) VMD – visual molecular dynamics. J Mol Graph 14:33–38
54. Oostenbrink C, Villa A, Mark AE, van Gunsteren WF (2004) A biomolecular force field based on the free enthalpy of hydration and solvation: the GROMOS force-field parameter sets 53A5 and 53A6. J Comput Chem 25:1656–1676
55. Schüttelkopf AW, van Aalten DMF (2004) PRODRG—a tool for high throughput crystallography of protein-ligand complexes. Acta Crystallogr D60:1355–1363
56. Böckmann RA, Hac A, Heimburg T, Grubmüller H (2003) Effect of sodium chloride on a lipid bilayer. Biophys J 85:1647–1655